INTERNATIONAL JOURNAL OF AUTOMOTIVE AND MECHANICAL ENGINEERING
ISSN: 2229-8649 e-ISSN: 2180-1606
VOL. 21, ISSUE 1, 2024, 10993 – 11009
DOI: https://doi.org/10.15282/ijame.21.1.2024.04.0850

RESEARCH ARTICLE

Enhancing Machining performance in Stainless Steel Machining using MXene Coolant: A Detailed Examination

M. Eaki[1], K. Kadirgama[1,2,3]*, D. Ramasamy[1], W.S.W. Harun[1], K.A. Abou-El-Hossein[4], L. Samylingam[5], and C.K. Kok[5]

[1]Faculty of Mechanical and Automotive Engineering Technology, Universiti Malaysia Pahang Al-Sultan Abdullah, 26600 Pahang, Malaysia
[2]Almaaqal University, College of Engineering, Department of Civil Engineering, Basra, 61003,Iraq
[3]Centre for Research in Advanced Fluid and Processes, Universiti Malaysia Pahang Al-Sultan Abdullah, 26600 Pahang, Malaysia
[4]Faculty of Engineering and Technology,Vaal University of Technology,Vanderbijlpark, South Africa
[5]Centre for Advanced Mechanical and Green Technology, Faculty of Engineering and Technology, Multimedia University, Jalan Ayer Keroh Lama, Bukit Beruang, 75450 Melaka, Malaysia

ABSTRACT - Metal cutting, a complex process in manufacturing, involves various factors that significantly affect the quality of the final product. Notably, the turning process is crucial, with outcomes that heavily depend on multiple machining parameters. These parameters encompass speed, depth of cut, feed rate, the type of coolant used (specifically, high heat transfer MXene coolant), and insert types, among others. The material of the workpiece is also a critical factor in the metal-cutting operation. This study focuses on achieving optimal surface quality and minimizing cutting forces in the turning process. It recognizes the substantial impact of numerous process parameters, directly or indirectly affecting the product's surface roughness and cutting forces. Understanding these optimal parameters can lower machining costs and improve product quality. Our research concentrates on turning a stainless-steel alloy workpiece using a carbide insert tool. We employ the Response Surface Method (RSM) to optimize cutting parameters within a set range of cutting speed (100, 125, 150 m/min), feed rate (0.1, 0.2, 0.3 mm/rev), and depth of cut (0.4, 0.8, 1.2 mm). Additionally, we use various tool geometries and the RSM design of experiments to enhance and analyze the multi-response parameters of surface roughness and tool life. Optimal machining parameters for MXene-NFC involve a cutting speed of 140 m/min, a feed rate of 0.05 mm/rev, and a depth of cut of 0.5 mm. These settings ensure minimal surface roughness, maximum tool life, and the greatest total length of cut, achieving a composite desirability of 0.695.

ARTICLE HISTORY
Received : 23rd May 2023
Revised : 17th Nov. 2023
Accepted : 02nd Jan. 2024
Published : 20th Mar. 2024

KEYWORDS
Stainless steel
Nanofluid
MXene
Surface roughness

1.0 INTRODUCTION

Martensitic Stainless Steel (MSS), acclaimed for its superior hardness, strength, and erosion resistance, plays a pivotal role in various design applications [1]. However, its low thermal conductivity challenges machining, leading to rapid wear on cutting tools. To counter this, MSS often uses cutting fluid to improve machinability, aiding in the machining process and debris removal. Despite their effectiveness, cutting fluids carry environmental and health hazards due to their synthetic chemical composition [1]. Their disposal is problematic and recycling them incurs considerable costs. Consequently, this research aims to reduce or eliminate dependence on cutting fluids, aligning with the modern manufacturing industry's shift towards "feasible machining." This concept emphasizes selecting appropriate cutting parameters and tool grades and minimizing cutting fluid use, prolonging tool life, improving surface finish, and boosting cutting efficiency. It also considers chip disposal, energy management, and atmospheric conditions, striving for optimized machining processes that are environmentally conscious and sustainable [2]. One approach to feasible machining is dry cutting, which eliminates cutting fluid use and prevents environmental pollution. However, dry machining faces increased friction and adhesion at the chip-tool interface, leading to faster tool wear [3]. This issue is addressed by applying protective coatings to cutting tools, enhancing performance through reduced friction and increased wear resistance. These coatings also slow heat transfer to the tool's forefront, extending its lifespan. Coating methods include Physical Vapor Deposition (PVD) and Chemical Vapor Deposition (CVD), with CVD preferred for multi-layered coatings [3]. Multi-layer coatings outperform single-layer ones. Notable layers include Titanium Carbide (TiC), Titanium Carbo Nitride (TiCN), Aluminum Oxide (Al_2O_3), Titanium Aluminum Nitride (TiAlN), and Titanium Nitride (TiN), each with unique properties. For example, TiN and TiCN reduce friction between tool and chip surfaces, while Al_2O_3 and TiC offer exceptional hardness and oxidation resistance. The key lies in optimising the coating structure and balancing material and thickness. Evaluating the cutting performance and wear behavior of novel cutting tools typically requires extensive testing, which is time-consuming and expensive. MXene's intrinsic hydrophilicity, when solution-processed, notably shows greater thermal and electrical conductivity than Graphene [4]. Its unique properties make it a promising material for further exploration in technological domains [4]. MXene as a nanofluid in machining requires detailed analysis, forming the core of this examination.

***CORRESPONDING AUTHOR | K. Kadirgama|** ✉ kumaran@ump.edu.my

2.0 MACHINING PROCESS TURNING

Turning is a fundamental machining operation, where a single-point cutting tool is maneuvered in alignment with the pivot direction [5]. The outer surface and interior of the part should both be amenable to turning, allowing for comprehensive machining. The initial material typically comprises various stages, including casting, fabrication, or extrusion [6]. Turning can be performed using both manual and computer-controlled, automated machines. Manual machines necessitate continuous oversight from the operator, whereas computer-controlled and automatic machines operate autonomously. The latter is commonly known as a Computer Numerical Control (CNC) machine and finds application across various machine tools, extending beyond the turning machine itself [7]. Straight turning, taper turning, profiling, and external grooving represent different turning processes. Workpieces with straight, conical, curved, or notched configurations can be manufactured through turning. The turning operation commonly employs single-point cutting tools. The materials of workpieces are classified based on established standards that have evolved [8]. Parameters such as cutting tool geometry, material composition, the frequency of tests conducted, depth of cut per pass, cutting depth, feed rates, cutting speeds, and the application of cutting fluids all play a significant role in shaping the generation of new and innovative outcomes [9]. These outcomes encompass Material Removal Rates (MRRs), tool lifespans, cutting power requirements, and machining characteristics such as surface roughness, circularity of rotations, and layered deviation of the workpiece in the turning process.

2.1 Cooling system in turning operation

Cutting fluid assumes a crucial role in conventional machining by effectively lowering the cutting temperature, prolonging tool life, minimising tool wear, and enhancing the dimensional stability of machined components [10]. Various cooling system application techniques, such as flood cooling, jet cooling, dry machining, and the minimum quantity lubrication technique, are commonly employed in machining processes.

Minimum Quantity Lubrication

The technique known as Minimum Quantity Lubrication (MQL) is considered more effective compared to similar methods, offering an alternative to dry machining by utilising a small number of coolants. Specifically, MQL involves a volume approximately three to four times smaller than the cutting fluids used in flooded conditions, typically at rates between 50–500 ml/h [11]. In this approach, the cutting liquid is atomised and directed to spray directly at the interface between the cutting tool and the workpiece. However, like the flood technique, the state of the cutting fluid differs significantly in each case. The heat generated during machining is dissipated through fluid evaporation. However, it's important to note that this application can lead to respiratory issues for machine operators [12]. The mist delivery of cutting fluid in this process risks workers' respiratory health. To mitigate these concerns, MQL can be implemented with cutting fluids that are non-toxic and biodegradable, thereby reducing the risk of respiratory problems. Furthermore, the application of MQL techniques contributes to a reduction in cutting fluid consumption [13]. Another term for the MQL concept is "near-dry lubrication," which is advantageous in minimising cutting liquid usage, consequently lowering overall production costs.

2.2 Machining parameters in the turning process

The process of creating machining plans for metal cutting involves various factors. Firstly, it is essential to comprehend the types of machining tasks that can be executed. Subsequently, understanding the machines capable of performing these tasks and the corresponding cutting devices becomes necessary. Lastly, a grasp of the parameters governing the cutting conditions, such as material properties and calculations, is crucial for executing these tasks effectively.

2.2.1 Process Parameters

- **Cutting rate** - This is the rate at which a machine removes metal from a piece of work material. Fringe speed is measured in m/min in a machine. In this equation, V is equal to the product of the cutting speed in revolutions per minute (rpm) divided by the length of the workpiece (in millimetres).
- **Depth of cut** (d): The opposing distance, measured in millimetres, between the machined surface and the whole area of the workpiece, is the profundity of the cut.
- **Spindle speed** - The workpiece and axle's rotating speed constantly change (RPM). The shaft speed is equal to the cutting speed, separated by the workpiece's edge.

Feed rate - Slicing device development is measured about the job piece as the slicing device cuts. It is measured in inches per minute (IPM) by combining both the cutting rate (IPR) and the thrust force (RPM).

2.2.2 Response Parameters

- A measure of the generation rate is the "material ejection rate," which is usually expressed in cubic inches per second. Increasing this rate will result in a section being completed more quickly, likely for less money. However, increasing the material evacuated rate typically increases equipment wear, helpless surface completions, helpless resilience and other concerns [14]. It is challenging to upgrade the machining process.

- The pace at which an instrument's cutting-edge erodes during machining is known as the device wear rate. The volume is usually expressed as a fraction of a cubic inch per second. The generation rate will fall as the pace of growth increases [15]. It will lead to the equipment wearing out.
- After a piece is manufactured, its surface is perfected to a certain degree by a process called "surface finishing." The roughness, waviness, and flaws that remain on the surface result from surface completeness. The surface roughness influences the wear resistance, erosion coefficient, and machined components' consumption resistance. Surface roughness may be affected by a variety of elements in real life, including the hardness of the workpiece, the cutting circumstances, and the kind of machinery used the device's substance, nose range, and rake point are examples of apparatus factors, others include state-of-the-art computation, instrument vibration and instrument point. etc [16].
- During machining, knowing how much cutting force is used is critical. Planned machine equipment elements and the machine body employ cutting powers. Workpiece deformation, layer accuracy, machine solidity, and chip development are all affected by cutting power. For the following reasons, it is vital to predict the quantity of powering down and how distinctive cutting boundaries influence cutting power even before starting up the machining activity.

2.3 Formation of build-up-edge

Due to the poor cutting speed, the build-up edge (BUE) may occur. These particles have been distorted and strain-hardened to a great degree. According to previous research, BUE is substantially more rigid than the workpiece material [17]. Research was conducted before to determine the possibility of BUE occurring during machining [18]. According to the findings of this inquiry, BUE only happens under the following circumstances [19]:

a) There is the occurrence of strain hardening on the material of the workpiece.

b) A chip formation that is steady and stationary.

c) A low temperature during chip creation prevents recrystallisation.

d) A stationary zone where material flows over the cutting edge.

The geometry of the cutting edge experiences the influence of BUE. Build-up edge can drag across the workpiece material during machining, leading to adhesive wear on the cutting tool and potentially compromising the integrity of the newly machined surface. Consequently, in machining processes, efforts are usually made to avoid the formation of this build-up edge. Nevertheless, an earlier experimental investigation has revealed that at high cutting speeds, the occurrence of the build-up edge is mitigated. This is attributed to the considerably higher recrystallisation temperature during the deformation process, which prevents strain hardening.

2.4 Tool life

Cutting fluids, capable of lubricating and cooling to reduce the heat around the cutting-edge zone, play a crucial role in achieving optimal results during machining. Originally, water served as the initial processing liquid in this context, contributing to the development of well-established machining theories. Over time, various emulsions, both with and without oil as the primary component, have been experimented with in research settings. These experiments have demonstrated significant enhancements not only in the surface quality of machined parts but also in prolonging machine life and optimizing conditions for the ejection of chips from the cutting zone, ultimately leading to improved accuracy in layered item production. Moreover, recent studies suggest the necessity of employing advanced machining fluids, particularly when dealing with challenging-to-machine materials [10]. Historically, flooded machining relied on machining liquids, utilizing approximately 1200 liters per hour as a dynamic medium, significantly escalating the production costs of components. However, the use of conventional oils and emulsions in this process posed significant threats to both human health and the environment due to the presence of harmful synthetic chemicals. Consequently, considerations related to health and finances, including the high expenses associated with machining fluid usage, have underscored the imperative to explore alternative solutions for wet machining. Alternative wet machining methods have emerged, notably through unique Minimum Quantity Lubricant (MQL) approaches. In the MQL technique, the dynamic medium comprises a blend of an oil-based emulsion concentrate and water, typically with a concentration ranging between 4% and 12%. As a primary cooling condition, lower temperature air is often employed as a substitute for water, reaching approximately 30 °C upon arrival at the cutting zone. Crucial components within the dynamic environment pertinent to MQL technology include mineral or vegetable oil. The consumption rates of machining liquids for these methods typically range between 10 and 200 ml/h during the metal cutting [20].

2.4.1 Mechanism tool wear turning

Due to the robust substance affinity of SUS 304, a primary concern during wear was the material bonding on the rugged tool surface. Material bonding on instrument surfaces resulted from workpiece materials undergoing thermal relaxation and visco-plastic streaming, as illustrated in Figure 1. EDS analysis, depicted in Figure 1, revealed distinct areas where thick membranous cement layers and exposed substrate instrument material were evident. The substance was so viscous in specific locations that the filtration device failed to identify instrument material components. Numerous flakes of SUS 304 adhered to the tool rake and flank surfaces during wear. In subsequent cutting phases, the coolant would replace the device materials, coming into direct contact with the workpiece and causing erosion. Given the prevalence of scraped area wear, the rake's equivalent grating imperfections resulted from repeated scratches on the

adhesive substance. This wear pattern indicated that the chip interface of the device played a role in overall scouring interaction, leading to more significant bonding and scraping area wear [21]. The cemented Mxene layers, to some extent, shielded the rake face from erosion caused by chips. The inconsistency and detachment of adhesive Mxene layers or exposed new device surfaces exposed the adhesive layers to continuous rubbing and damage from chipping [22]. When these adhesive layers reached a certain inertia threshold, they became unstable. The substance intermittently detaches under the shear strain of flowing chips, leaving behind a torn surface. Mxene was bonded to have a similar surface to speed up the wear process. According to this wear cycle, the process of "arrangement aggregation (the creation of grip layers)- stripping off" may be summarised. Cement platinum layers were found on the instrument's rake face and flank face, as seen in Figure 1. A wedge-like effect was created because the adhesive Mxene was continuously deposited layer by layer.

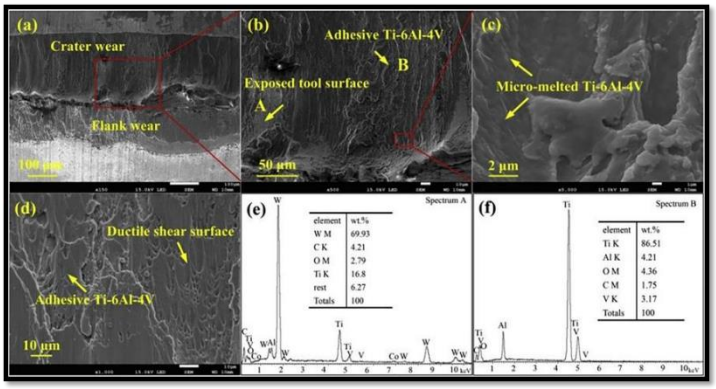

Figure 1. Wear surface morphology of crater wear and flank wear at v = 50 m/min, VB = 0.3 mm

3.0 PREPARATION NANOFLUIDS

The prepared MXene-NFC will be stirred using a magnetic stirrer for 30 minutes. The purpose of this stirring process is to make sure the MXene-NFC is thoroughly mixed and becomes uniform. Scientists evaluated the thermal conductivity of nanofluids using various liquids and nanoparticles, employing the transient hot wire technique, as stated in ASTMD 2717. This method involves essential components such as an information security framework, a digital signal converter, the Wheatstone Bridge, and other devices. Optionally, a nanofluid transporter and chiller are incorporated. The circuit includes variable opposition (Rd), while Rc provides fixed resistance. Rw represents a cryptic opposition, and Rd can be utilised to assess the value of other obstructions. To experiment, an isotropic liquid is poured over a thin wire serving as the heat source. A constant, warm spray around the liquid compartment ensures temperature stability, and the wire length is theoretically infinite. The wire used for exploration is immersed in nanofluid, providing heat and temperature readings. The temperature of both the wire and the liquid increases due to the wire's heat. The heated conductance of the liquid contributes to the rise in the wire's temperature. Various methods, such as the warm constants analyzer approach, the steady equal plate methodology, and the three strategies, are employed to estimate nanofluid thermal conductivity. A rotational rheometer is commonly employed to determine the viscosity of nanofluids, utilizing rheometers or viscometers. In specific instances, rheometers of the circular chamber/axle type or the cones and plate type are employed in conjunction. Instruments such as the vibro viscometer and hair-like structures viscometer, among others, have not been extensively studied to determine nanofluids' consistency. Various factors, including molecule shape and size, the size and volume of nanomaterials present in the liquid, and the use of surfactants, can influence the overall viscosity of nanofluids. Different-sized equivalent nanoparticles exhibit varying viscosity in nanofluids. Traditionally, nanofluid consistency has been associated with the size of molecules in the fluids. Despite this, few studies have reported a decrease in consistency with an increase in molecule size. Nanoparticles with a smaller surface-to-volume ratio experience more extensive blockage at the nanoparticle-liquid point of contact, decreasing consistency. The thickness of nanofluids has been demonstrated to be strongly influenced by the condition of the distributed nanomaterial. Based nanofluids with stretched particles exhibit expanded consistency compared to nanofluids with spherical nanoparticles, as reported by Mia, Bashir [20]. There has been a widespread finding that volume convergence in nanofluids has an increasing effect when even a tiny volume component of nanomaterial expands. The most significant influence on nanofluid consistency is temperature. As the temperature rises, the force inside the particles and liquid decreases, as shown by [23], and as a result, the consistency decreases. There is a similar pattern of thickness abatement with temperature expansion when looking at the nanofluid of zirconia nanoparticles and alumina in ethylene glycol nanofluids. In addition to thickness, the nanofluid's pH is another characteristic that has shown a correlation. According to research, the nanofluid scattering is stable at a certain pH value. Using Wang, Li [24] a review, nanofluids with the most negligible viscosity comprising alumina and copper nanoparticles were identified in the pH range of 7.7 - 8.9 for alumina and >7.6 for copper nanoparticles. Additionally, the shear rate distinguishes between Newtonian and non-Newtonian nanofluids, directly influencing the latter's thickness. The thickness of nanofluids depends on many additional barriers; yet, there is no possible equation to measure the consistency of a nanofluid correctly. After that, new models must be developed to determine nanofluids' thickness accurately [25]. The equipment that used in measurements is shown in Figure 2, 3 and 4

Figure 2. Magnetic stirring process

Figure 3. Ultrasonic bath sonication process

Figure 4. Viscometer device [26]

3.1 Experimental selection of cutting data

The experimental design comprises two phases: preliminary and final. During the preparatory stage, the aim is to identify suitable cutting speed, feed rate, and axial depth ranges. Subsequently, in the final phase, a comprehensive analysis of the cutting tool material is conducted, and the outcomes of earlier tool tests inform this selection. Determining the optimal combination of machine tools, cutting tools, and conditions is a resource-intensive and time-consuming process. To streamline this, the decision was made to employ the design of experiment (DOE) approach. This involves identifying a potential range of cutting conditions for the cutting tool based on the outcomes of preliminary tests conducted with various cutting tools at different parameters. By utilising response surface methodology (RSM), it becomes possible to minimise the time and costs associated with selecting the best tool and cutting conditions, thereby maximizing the material removal rate.

3.1.1 Cutting speed

When a cutting speed is referred to, it means the linear movement speed between the tool and the workpiece. As previously indicated, three cutting speeds are available: high, medium, and low. The cutting tool supplier's recommended range of cutting speed for SUS 304 stainless steel is used to determine the flank wear criterion for the tool.

a) 120 m/min
b) 140 m/min
c) 160 m/min

3.1.2 Feed rate

As the cutting tool moves about the workpiece, it is called tool feed. The millimetre per tooth (mm/tooth) unit of measurement is used. Feeds were arranged in the following manner:

a) 0.05 mm/rev
b) 0.10 mm/rev
c) 0.15 mm/rev

3.1.3 Depth of cut

The depth of cut is the distance between the bottom of the cut and the uncut surface of the workpiece measured in a direction at right angles to the machined surface. The depth of cut levels which have been selected were 0.5 mm, 1.5 mm, and 2.0 mm. The three levels are as follows:

a) 0.5 mm

b) 1.25 mm

c) 2.0 mm

3.2 Design of Experiment (DOE)

The Response Surface Method (RSM) was selected for implementation in conjunction with the Design of Experiments (DOE). This approach provides a robust framework for exploring the relationships between multiple independent variables and one or more response variables. The suitable levels of the factors are used to deduce the design parameters for sus 304 stainless steel, shown in Table 1. The lower and higher speed values selected were 120 m/min and 160 m/min, respectively. The feed rate, and depth of cut are 0.05 to 0.15 mm per revolution and 0.5 to 2 mm, respectively. Table 2 shows the selected values for the variables.

Table 1. The values selected for the variables

Factors/Coding of Level	-1	0	1
Speed, Vc (m/min)	120	140	160
Feed rate, f (mm/rev)	0.05	0.10	0.15
Depth of cut, d (mm)	0.5	1.25	2.0

Table 2. The design values

Experiment Number	Cutting speed, Vc (m/min)	Feed rate, f (mm/rev)	Depth of cut, d (mm)
1	140	0.10	1.25
2	120	0.10	2.00
3	140	0.15	2.00
4	120	0.15	1.25
5	160	0.10	2.00
6	120	0.05	1.25
7	140	0.10	1.25
8	160	0.05	1.25
9	160	0.10	0.50
10	140	0.05	0.50
11	140	0.15	0.50
12	140	0.05	2.00
13	120	0.10	0.50
14	140	0.10	1.25
15	160	0.15	1.25

3.3 Workpiece material

As illustrated in Figure 5, the metal workpiece utilised in this investigation is SUS 304 stainless steel rod from ASSAB Steel (M) Sdn. Bhd. The rod has a diameter of 32 mm and a length of 120 mm. This block's hardness is Rockwell B 103. Table 3 displays the chemical compositions. Table 4 shows the physical parameters of the workpiece material.

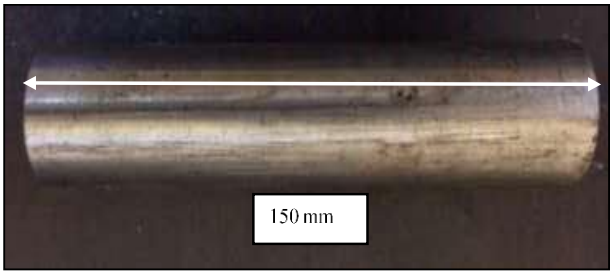

Figure 5. Workpiece material

Table 3. Chemical composition of workpiece material

Element	C	Si	Mn	Cr	Mo	Cu	Co	Ni	Mo	Fe
Wt %	0.0669	0.621	1.44	17.800	0.147	0.555	0.212	8.320	0.461	70.2

Table 4. Physical properties of workpiece material

Properties	Value
Density (kg/m^3)	7880
Elastic Modulus (GPa)	193.0
Thermal Expansion Coefficient ($^oC^{-1}$)	0.0000174
Thermal Conductivity at 100^{o}C	15.1
Thermal Conductivity at 500^{o}C	19.4
Specific Heat (J/kg.K)	496

3.4 Lathe machine

The Pinacho S90VS 180-750/1000 machine, a typical lathe, was employed for the turning experiment. A 4.0-kilowatt electric motor powered this piece of machinery. With a maximum spindle speed of 2500 RPM, this is a manually operated machine with dimensions of 1485x950x2170 mm. Figure 6 depicts the lathe machine utilised in the turning experiment. The Pinacho S90VS 180-750/1000 machine's specifications are shown in Table 5.

Figure 6. Pinacho S90VS 180-750/1000 lathe machine

Table 5. Specification of Pinacho S90VS 180-750/1000 lathe machine

Specification	Value
Centre height	180 mm
Centre distance	750 - 1000 mm
Swing over bed	360 mm
Swing over gap	520 mm
Swing over carriage	335 mm
Swing over cross slide	205 mm
Bed width	250 mm
Gap length in front of face plate	130 mm
Main spindle bore	42 mm
Main spindle nose	DIN 55027 No.5 CAMLOCK No.5
Main spindle taper	4 MT
Speed range	I: 0 - 310 RPM II: 310 - 890 RPM III: 890 - 2500 RPM
No. of speeds	variable
Main motor power	4 kW
Pump motor power	0.06 kW

3.5 Minimum Quantity Lubrication (MQL)

Using the right amount of lubricant for each machining process is critical while using a minimum quantity lubrication. The Unist Coolubricator, as illustrated in Figure 7, is employed to supply nanofluid-based cutting fluid in this study. With an adjustable positive displacement pump and precise air metering adjustment, the Unist Coolubricator constantly supplies cutting fluid. This Coolubricator is made up of a container that can hold up to 1800 ml of cutting fluid for turning

operations. Aside from that, the Coolubricator's pump may have an output ranging from 0.03 ml per stroke to 0.1 ml per stroke.

Figure 7. Unist Coolubricator

3.6 Surface roughness tester

The surface roughness of the workpiece after machining is measured using a low-weight portable surface roughness tester type Elcometer 7061 MarSurf PS1. This device determined the arithmetic average surface roughness (Ra) and mean roughness depth (Rz).

3.7 Optical measuring device

The cutting tool's tool wear was measured using the Knoop/Vickers Tukon 1202 Hardness Tester. For quick and straightforward positioning and focusing, this gadget has three magnification settings: 5 X, 10 X, and 50 X. Aside from that, the Tukon 1202 is entirely compatible with MinutemanTM camera systems

3.8 Experiment Setup Preparation

To begin the experiment, the SUS 304 stainless steel rod was sanded to a 240 grit finish, effectively removing any visible dust particles from the surface of the workpiece. A final turning operation followed this to ensure the surface stability of the workpiece. Before testing, all cutting inserts were inspected and found to be issues-free. The cutting tool was then securely fastened to the holder using a clamp. The evaluation of the cutting tool's effectiveness was limited to examining only one side of the inserts. In preparation for the experiment, the machine table was cleaned with a cloth to ensure the stability of the workpiece during the process. An additional tool holder was mounted on the tool post using a clamp, and the insert-equipped tool holder was then attached to this additional holder. The height of the additional holder was adjusted to align the insert tip with the centerline tip at the dead stock and then tightened into position. The initial step involved securing the workpiece rod in the chuck. The cutting depth was set, and the cross-slide handle wheel was used to adjust the cutting height. The feed rate was then modified using the lathe gears, as the machine's catalogue specified. The spindle's cutting speed was fine-tuned by adjusting the knob, followed by closing the headstock's cover to commence machining. The turning process was repeated to complete a single 80 mm length cut. After each pass, the cutting tool and workpiece were unclamped to assess the insert's flank wear and the surface roughness of the workpiece. Three readings were taken at the turning area to calculate the average surface roughness. The workpiece was rotated to collect surface roughness data at three different positions, and the average surface roughness was determined from these readings (Ra1 through Ra3). Simultaneous measurements of surface roughness and flank wear were carried out. Flank wear was measured as the distance from the original cutting edge to the boundary of the wear land after each round. Following the ISO 3865:1977 standard, which recommends a cutting insert wear limit of 0.3 mm for turning, side wear was recorded after each pass until this specified wear limit was reached. Tool holders and inserts were checked and retightened to begin another pass if necessary.

4.0 EXPERIMENTAL RESULTS

4.1 Evaluation of nanofluid stability

Single-layer nanoparticles are first created by dissolving multi-layer MXene-Ti_3c_2tx nanosheet powder in vegetable oil at varied concentrations (0.01g, 0.03g and 0.5g of MXene powder) and then dissolving it in vegetable oil. Using a fresh, centrifuged mag-strimmer, the solution was swirled for half an hour at room temperature (5 min, 3500 rpm). MXene-NFC solution was ultrasonically treated at 20 kHz for 60 minutes to further breakdown force molecules between

multilayered Ti3c2Tx nanoparticles. Multi-layered Ti3c2Tx nanoparticles are delaminated into single-layered nanoparticles by ultrasonic treatment of the solution. In the end, just the base liquid's thermal conductivity and viscosity were assessed

4.2 Thermal conductivity of nanofluid

The MXene-NFC of various volume concentrations is prepared, and the thermal conductivity is measured. The volume concentrations that have been tested are 0.1%, 0.3% and 0.5%. The concentrations arrived from the DOE done for the best-measured concentrations. The thermal conductivity has been measured at six distinct temperatures, which are 30 ºC, 40°C, 50 ºC, 60°C,70°C and 80 ºC. The experimental data is recorded on the effectiveness of the coolants. Figure 8 shows the thermal conductivity reading of conventional MXene-NFC of various volume concentrations.

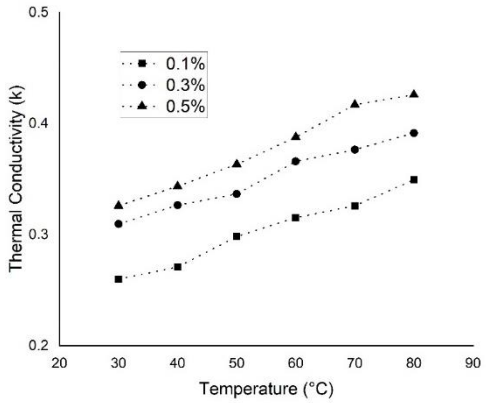

Figure 8. Thermal conductivity of various volume concentration

The relationship between temperature, volume concentration, and thermal conductivity is depicted in Figure 8. Notably, the highest thermal conductivity value was observed at a temperature of 80°C and a volume concentration of 0.5 percent. Conversely, the lowest thermal conductivity rating occurred at 30°C and a volume concentration of 0.1 percent. Figure 8 illustrates that the thermal conductivity of MXene-NFC surpasses that of its base fluid. This phenomenon could theoretically be elucidated through the principles of Brownian motion [16, 27, 28]. As the temperature increases, particles experience more frequent collisions and carry greater kinetic energy, resulting in an elevation of thermal conductivity. A similar thermal property behavior is observed in the Fe_3O_4 nanofluid, a combination of ethylene glycol and water [29]. The depicted figure indicates a positive correlation between thermal conductivity and volume concentration. This is attributed to the heightened Brownian diffusion rate, contributing to an overall increase in the material's thermal conductivity. Consequently, it is inferred that the heat absorption capacity of 0.5 percent MXene-NFC, containing MXene, surpasses that of 0.1 percent MXene-NFC, particularly at the interface between the workpiece and cutting tool. The exceptional thermal conductivity of MXene-NFC significantly aids in dissipating the heat generated during machining. Notably, the thermal conductivity of MXene-NFC nanofluid surpasses that of traditional metalworking fluid (MWF), as previously demonstrated [30].

4.3 Viscosity of nanofluid

The nanofluid of various volume concentrations is prepared and the viscosity is measured. The volume concentrations that has been tested is 0.1%, 0.3 % and 0.5 %. The viscosity has been measured at three distinct temperature which are 30 ºC, 40 ºC, 50 ºC, 60 ºC, 70 ºC and 80 ºC. The experimental data is recorded and compared the effectiveness of the coolants. Figure 9 shows viscosity reading of conventional MXene-NFC of various volume concentration.

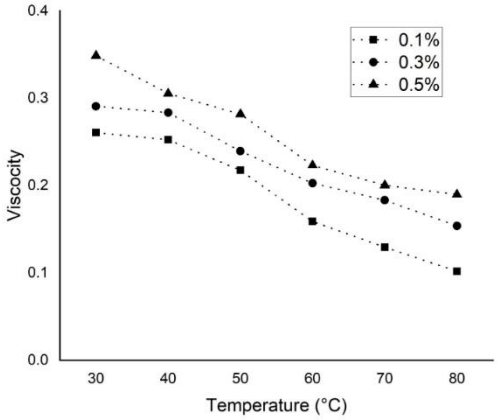

Figure 9. Viscosity of various volume concentration

The results presented in Figure 9 reveal a decrease in viscosity with increasing temperature and an increase with higher volume concentration. The maximum viscosity value was observed at a temperature of 30°C and a volume concentration of 0.5%, while the minimum viscosity occurred at 80°C and a volume concentration of 0.1%. The decline in viscosity with rising temperature can be attributed to the weakening of interparticle and intermolecular adhesion forces within the nanofluid [31]. This leads to an expansion of the free volume in the nanofluid structure and a subsequent decrease in internal friction forces between molecules. Conversely, an increase in volume concentration results in higher viscosity due to its impact on the internal shear stress of the fluid. The specific findings indicate that a concentration of 0.5% MXene results in lower viscosity compared to a concentration of 0.1% MXene. A fluid with lower viscosity is more suitable for use as a machining coolant. This is because a fluid with lower viscosity requires less power consumption by the pump. Consequently, a cooling system with lower power consumption is more convenient, especially in Minimum Quantity Lubrication (MQL) systems where the pump circulates or delivers coolant from the storage tank.

4.4 Nanofluid Selection

As an alternative coolant to traditional machining coolants, nano fluids used as coolants must have better thermal conductivity and lower viscosity. Figure 9 shows that all MXene-NFC volume concentrations containing MXene have greater thermal conductivities. Only 0.5% of the total volume of MXene-NFC has a lower viscosity. This research used MXene-NFC at a volumetric concentration of 0.5 percent because it increased thermal conductivity more than other MXene-NFC solutions while decreasing viscosity. Higher heat conductivity and lower viscosity values were also reported by the MXene-NFC that was used for this study. MXene-NFC was thus tested in round operation at a 0.5 percent volume concentration to assess its machining efficiency in comparison to MWF

4.5 Responses Model

The linear model shows the relationship between the turning response and the independent variable can be represented as following expression:

$$y' = (Cutting\ speed) + b(Feed\ rate) + c(Depth\ of\ cut) + D \quad (1)$$

where *a, b, c and D* are the constants. Eq. (1) can be expressed in the following form:

$$y'' = \beta_0 x_0 + \beta_1 x_1 + \beta_2 x_2 + \beta_3 x_3 \quad (2)$$

where y = turning response, x_0 = 1(dummy variable), x_1 = cutting speed, x_2 = feed rate, x_3 = depth of cut. β_0, β_1, β_2 and β_3 are the model parameter. The second-order model can be expressed as:

$$y'' = \beta_0 x_0 + \beta_1 x_1 + \beta_2 x_2 + \beta_3 x_3 + \beta_4 x_1^2 + \beta_5 x_2^2 + \beta_6 x_3^2 + \beta_7 x_1 x_2 + \beta_8 x_1 x_3 + \beta_9 x_2 x_3 \quad (3)$$

4.6 Development of Surface Roughness Model of MWF Coolant and MXene-NFC

After the first pass of turning experiment which is 80 mm of cutting, the surface roughness reading is used to generate the full quadratic model Eq. (3). In order to calculate this parameter, the response surface method is used with aid of Minitab Software. The linear equation is used to predict the surface roughness of TURNING experiment conducted with MWF AND MXene-NFC is expressed as:

Surface roughness using metal working fluid (MWF) coolant =

$$10.69 - 0.1230x_1 - 15.47x_2 - 0.300x_3 + 0.000370x_1^2 + 10.0x_2^2 - 0.3305x_3^2 + 0.0790x_1x_2 + 0.00857x_1x_3 + 0.93x_2x_3 \quad (4)$$

Surface roughness using MXene-NFC =

$$11.30 - 0.1373x_1 - 18.67x_2 - 0.227x_3 + 0.000433x_1^2 + 17.5x_2^2 - 0.3062x_3^2 + 0.0838x_1x_2 + 0.00702x_1x_3 + 1.47x_2x_3 \quad (5)$$

In the context of rotating operations employing standard machining coolant (MWF) and MXene-NFC, it is evident from Eqs. (4) and (5) that the feed rate exerts the most substantial influence on average surface roughness, followed by cutting depth and cutting speed. This observation aligns with the findings of [32], reinforcing the patterns illustrated in Eqs. (4) and (5). Surface roughness is most significantly impacted by the feed rate. The increase in feed rate results in heightened frictional forces between the cutting tool's edges and the workpiece, as the tool swiftly traverses the workpiece orthogonally. This escalation in frictional force amplifies the heat at the cutting tool's interphase. Consequently, the material's shear strength diminishes, causing deformation in the workpiece due to its ductility. Given that stainless steel exhibits ductile characteristics, the surface of the workpiece becomes adhesive, contributing to an elevation in surface roughness. The cutting depth stands as the second most influential factor affecting surface roughness, as indicated by Eqs. (4) and (5). This correlation stems from the concurrent escalation in cutting force associated with increased cutting depth, facilitating high vibration and natural frequencies. Lowering the cutting depth in metal cutting processes minimizes both cutting force and the effects of vibration and natural frequency, ultimately resulting in a smoother finish [33]. In comparison to the feed rate and depth of cut, cutting speed exerts the least impact on surface roughness. As cutting speed increases, the mean surface roughness decreases. This is attributed to the diminished likelihood of a build-up edge (BUE) with higher cutting speeds. Consequently, a cutting tool with less BUE produces a finer surface finish.

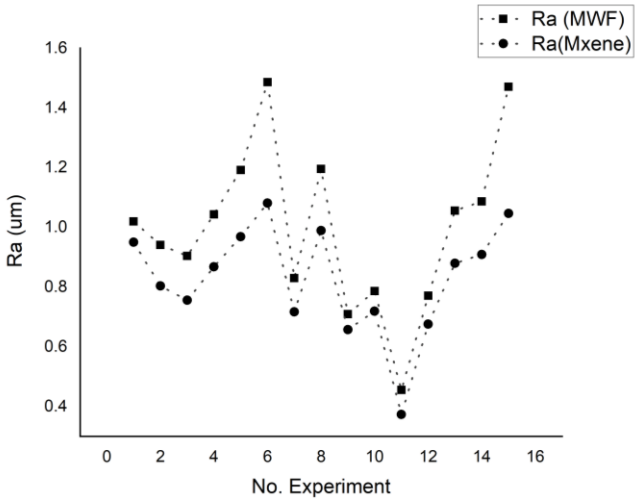

Figure 10. Experimental results for surface roughness using MWF and MXENE-NFC

4.7 Optimization of Surface Roughness Value

To optimize the surface roughness value, a reaction optimizer was used [34]. The optimum value of surface roughness corresponds to linear model design for MWF turning experiment is 0.953 µm with cutting speed = 160 rpm, feed rate = 0.10 mm/tooth and axial depth of cut = 0.5 mm (Figure 10). Meanwhile, the optimum value of surface roughness corresponds to linear model design for MXene-NFC turning experiment is 0.622 µm with cutting speed = 160 rpm, feed rate = 0.10 mm/tooth and axial depth of cut = 0.5 mm.

4.8 Development of linear tool life model with MWF and MXene-NFC

Field and Kahles, 1971 stated that tool life can be found from the expression below:

$$Tool\ life = TL/Fm \tag{6}$$

where *Fm* is the feed rate in mm/min and *TL* is the total length to reach flank wear criterion 0.3 mm.

The linear equation used to predict the tool wear for turning with water soluble coolant and nanofluid can be expressed as [35]:

Water soluble coolant

$$Tool\ life = -0.0096x_1 - 650.25x_2 - 0.205x_3 + 55.94 \tag{7}$$

Nanofluid

$$Tool\ life = -0.0166x_1 - 1181x_2 - 4.488x_3 + 55.94 \tag{8}$$

The longevity of the cutting tool experiences an upturn as cutting speed, feed rate, and axial depth of cut witness a reduction, as demonstrated by Equations 6 and 7 [36]. Among these factors, feed rate emerges as the most crucial determinant of tool life, closely followed by depth of cut and cutting speed. Consequently, enhancing turning tool life involves the strategic combination of low cutting speed, low feed rate, and low axial depth of cut. This aligns with the findings reported by [37] which emphasize that elevating cutting speed, feed rate, and axial depth of cut tends to diminish tool life. Moreover, tool life exhibits a consistent decline with escalating cutting speed, according to [38]. In Contrast, Koshy, Dewes [39] arrived at a similar conclusion using a linear model, contending that cutting speed exerts only minimal influence on tool life, particularly for hardened steel workpieces. The root cause of this phenomenon lies in the heightened temperatures experienced in the main and secondary shear zones. Elevated temperatures are often responsible for various forms of tool wear, including plastic deformation. Consequently, these temperature-related variables contribute to the deterioration of the cutting tool material, ultimately leading to its failure.

As the tool engages in cutting operations, its cutting edge gradually experiences wear over time [40]. Interestingly, both studies underscore that increasing cutting speed contributes to an extension in tool life. As elucidated by [41] , elevated cutting speeds reduce the contact area between chip-tool interfaces, leading to concentrated high temperatures near the cutting tool's edge. This heightened temperature compromises the strength of the cutting tool, resulting in plastic deformation. Moreover, the increased thermal gradient accentuates tool wear, given the escalated rate of thermal crack development [42]. Remarkably, a noteworthy observation is the substantial increase in tool life when the axial depth of cut is reduced. In both experiments, augmenting the axial depth of cut has minimal impact on tool life. This observation aligns with the findings of [43] , who posit that a significant increase in the axial depth of cut should not notably influence the rate of tool life. Previous studies indicate that as the axial depth of cut rises, the contact stresses at the tool-chip interface increase, while the average temperature remains relatively stable. Consequently, under optimal conditions of feed rate and cutting speed during the turning operation, a high axial depth of cut is unlikely to affect the tool life rate.

However, it is essential to acknowledge that several studies have demonstrated that increasing the axial depth of cut can curtail tool life by accelerating abrasion, adhesive, and diffusional types of tool wear [44].

This underscores the efficacy of utilizing MXene-NFC nanofluids as coolants in enhancing the overall lifespan of machining tools. The significant reduction in tool wear observed with MXene-NFC nanofluids, as opposed to traditional MWF, can be attributed to the exceptional heat transport capabilities of nanofluids at the tool-chip interface. Elevated temperature concentrations at the edges of the ribs typically result in a higher wear rate. However, the utilization of nanofluids as cutting fluids serves to mitigate this concern by reducing the penetration of temperature into the cutting tool, thanks to the high heat transfer rate characteristic of nanofluids. The relatively large surface area of nanoparticles further augments the heat transfer capacity, given that heat transfer primarily occurs at the particle surface [45]. In contrast, It is noteworthy that an increase in cluster size leads to a higher weight of nanoparticles in the base liquid, thereby increasing the likelihood of deposition and compromising nanoparticle stability. As highlighted by Murshed, De Castro [45] the gravity of nanoparticles becomes insignificant when the cluster size is small. However, excessive clustering in base liquids can impede the Brownian motion of nanoparticles, diminishing the rate of heat transfer.

4.9 Analysis of tool wear on turning performance using MWF and MXene-NFC

The fluctuation in flank wear breadth increasing metal cutting distances in the turning process of SUS 304 stainless steel utilising MWF coolant with MXene-NFC is shown in Table 6 and 7 [36]. According to the findings, flank wear rises as the length of the incision grows. In his research on tool wear of AISI 304 during turning operations, [46] found a similar tendency. The cutting tool can cut a SUS 304 stainless steel workpiece for a total length of 80 mm in each pass. The flank wear will be measured after each pass, and the turning process will be repeated until the wear meets the ISO 3865:1977 wear requirement of 0.3 mm flank wear. Cutting parameter No.15 (cutting speed = 160 m/min, feed rate = 0.15 mm/rev, and depth of cut = 1.25 mm) had the greatest flank wear rate when compared to other cutting parameters in the MWF coolant experiment. For cutting parameter No.15 (cutting speed 120 m/min, feed rate 0.05 mm/rev, and depth of cut = 1.25 mm), the flank wear reached tool wear criteria at around 24 mm total length of cut, whereas for cutting parameter No.6 (cutting speed 120 m/min, feed rate 0.05 mm/rev, and depth of cut = 1.25 mm), the cutting tool reached tool wear criteria at around 71 mm total length of cut. The impact of cutting speed and feed rate on flank wear is described here. The greater the cutting speed and feed rate, the more the flank wear rises. According to [47], the increased creation of heat during the metal cutting process at higher cutting speeds affects the flank wear development on the cutting tool. As a result, the tool's cutting edge softens at high temperatures during the metal cutting process in the tool-chip interphase, resulting in progressive wear.

In contrast, replacing MWF coolant with MXene-NFC enhanced the overall length of cut during turning operations on SUS 304 stainless steel workpieces with equal cutting settings [48]. Cutting parameters No.15 and No.6 have a significant increase in total cut length to meet the ISO 3865:1977 wear requirement under the same cutting circumstances. For cutting parameters No.15 and No.6, the flank wear reaches the wear criterion approximately 80 mm and 240 mm of total cut length, respectively. As a result, MXene-NFC has a strong hold on the flank wear rate for turning metal cutting operations involving hard materials like SUS 304 stainless steel. Vasu and Pradeep Kumar Reddy [49] found a similar outcome when they used MXene-NFC as a coolant and found that tool failure was delayed. The MXene-NFC is capable of carrying away a larger quantity of heat produced during the turning process because to its better thermal conductivity qualities [50]. The improved qualities of nanofluid allow the cutting tool's hardness to be retained and the time it takes to meet the failure wear criterion to be extended.

Table 6. Progression of flank wear by total length of cut for turning using MXene-NFC

Experiment Number	80 mm	160 mm	240 mm	320 mm	400 mm	480 mm
1	0.221	0.347	-	-	-	-
2	0.324	-	-	-	-	-
3	0.351	-	-	-	-	-
4	0.1519	0.2729	0.3578	-	-	-
5	0.319	-	-	-	-	-
6	0.412	-	-	-	-	-
7	0.249	0.412	-	-	-	-
8	0.258	0.396	-	-	-	-
9	0.052	0.127	0.237	0.297	0.349	-
10	0.048	0.118	0.215	0.254	0.319	-
11	0.045	0.106	0.183	0.249	0.272	0.327
12	0.437	-	-	-	-	-
13	0.134	0.276	0.365	-	-	-
14	0.346	-	-	-	-	-
15	0.312	-	-	-	-	-

Table 7. Progression of flank wear by total length of cut for turning using MWF

Experiment Number	80 mm	160 mm	240 mm	320 mm
1	0.231	0.354	-	-
2	0.436	-	-	-
3	0.671	-	-	-
4	0.239	-	-	-
5	0.519	-	-	-
6	0.452	-	-	-
7	0.269	0.395	-	-
8	0.598	-		-
9	0.092	0.187	0.325	-
10	0.072	0.159	0.287	0.412
11	0.075	0.157	0.269	0.382
12	0.757	-	-	-
13	0.184	0.325	-	-
14	0.379	-	-	-
15	0.338	-	-	-

4.1 Analysis of wear mechanism on Turning Performance Using MWF and MXene-NFC

Furthermore, the spectral data collected from EDX may be utilised to define the kind of wear that occurs on the cutting insert's rake face. Figure 11 provides a depiction of the microscope rake face for worn inserts exposed to rotation along an 80 mm axis, with nanofluid at 140 rpm, a feed rate of 0.05 mm/tooth, and an axial depth of 2.00 mm. The spectrum notably reveals a peak in iron (Fe), a crucial observation during turning and indicative of iron-built-up edge (BUE) formation that occurs when nanofluids are employed in the turning process [51]. Moreover, in accordance with [52], it's important to note that BUE generation is typically associated with the machining of ductile materials like austenitic stainless steels, particularly at low cutting speeds. Elements such as chromium (Cr), manganese (Mn), sulfur (S), silicon (Si), nitrogen (N), and oxygen (O) are also distinctly visible in the spectrum. Many of these elements are alloying components present in AISI 304 stainless steel, commonly used in the production of workpieces. The presence of these elements is attributed to diffusion wear, occurring at the tool-chip contact, where workpiece components are transported to the insert rake face. During the machining process, carbon and metal particles, in the form of chips, are transferred to the insert rake face [53]. At this juncture, the atoms of the workpiece's alloying elements react with the insert coating, contributing to further degradation of the rake face [53]. According to a prior study by Jawaid, Sharif [54], corrosion wear involves the loss of tool material granules or agglomerates due to intermittent tool-workpiece adhesion resulting from uneven chip flow and semi-stable BUE rupture. Shear wear, on the other hand, is associated with the significant acceleration of tool particles during the machining of steel materials. This behavior is characterized by the cyclic adhesion and removal of workpiece and chip material from the tool, as well as the removal of tool particles [55].

Turning experiments employing a nanoparticle-based coolant (TiO_2/EG) reveal a micro-wear mechanism, a phenomenon common in many cutting inserts. However, this Built-Up Edge (BUE) is not stable, as observed [56]. The clear deposition of workpiece material on the face of the turning insert rake is evident in Figure 12, showcasing the occurrence of adhesion when the coating emerges from the worm, according to [57]. Following the removal of the TiN-coated layer, the adherence of workpiece material to the rake face of the turning insert creates a robust shield on the insert layer. Additionally, as depicted in Figure 13, attached Ti nanoparticles impact and infiltrate the insert surface, precipitating as a metal layer. Proof of this is observed when the EDX spectrum exhibits a peak in Ti metal. The adhesive layer, comprising Ti nanoparticles, serves as an additional protective layer for the cutting inserts. Post-tool failure, the adhering metal is typically found on the rake face rather than the wing face. Despite the reduction in cutting temperature at the workpiece interface achieved by using nanoparticle-based coolants (TiO_2/EG) during the manufacturing process, oxidation still occurs. According to [58], the extraction of an O atom from a water-soluble coolant (H_2O) is a crucial chemical step in wear oxidation due to its lack of unpaired d-electrons. This suggests that milling with nanoparticle-based coolants (TiO_2/EG) induces oxidative wear. A small quantity of oxygen from the coolant (40 percent water, 60 percent EG) reaches the workpiece interface during the production process. The resulting oxidation layer is resilient, challenging to peel away from the tool surface, and becomes an integral part of the tool material when subjected to high turning forces. This phenomenon protects the tool against micro-cracking and debris wear.

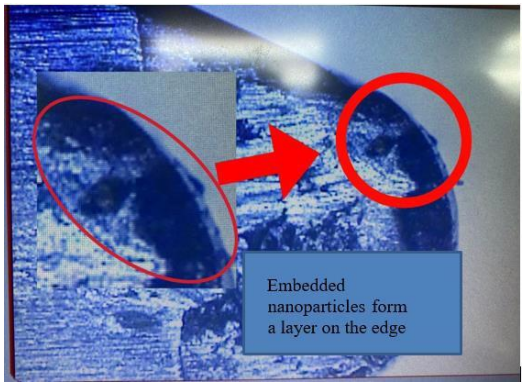

Figure 11. Microscope of cutting edge at cutting speed 140 rpm, feed rate 0.05 mm/tooth, axial depth 2.00 mm under nanofluid MXENE-NFC coolant at 80 mm of cutting distance

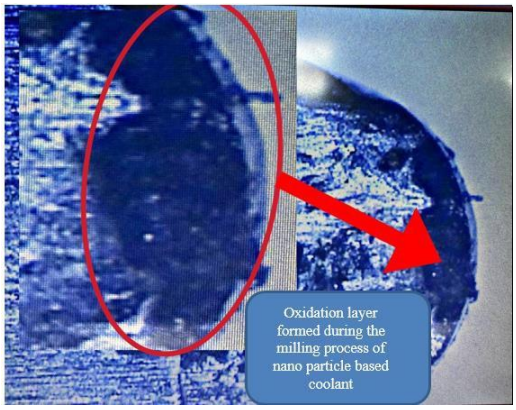

Figure 12. Microscope of cutting edge at cutting speed 120 rpm, feed rate 0.05 mm/tooth, axial depth 1.25 mm under nanofluid MXENE-NFC coolant at 80 mm of cutting distance

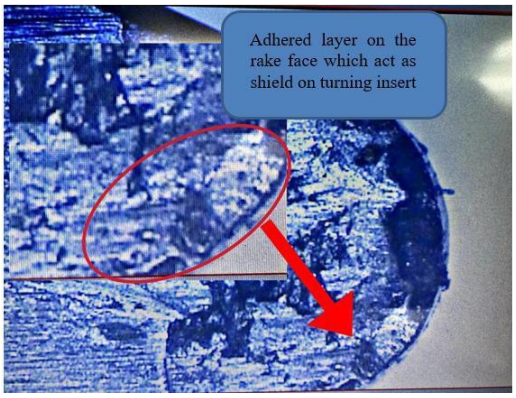

Figure 13. Microscope of cutting edge at cutting speed 160 rpm, feed rate 0.05 mm/tooth, axial depth 1.25 mm under MXENE-NFC coolant at 80 mm of cutting distance.

5.0 CONCLUSIONS

Throughout this research, MXene-NFC has demonstrated superior effectiveness compared to traditional machining coolant (MWF) within the Minimum Quantity Lubrication (MQL) cooling system. The evaluation encompassed thermo-physical qualities, including heat conductivity and dynamic viscosity, as well as the performance of turning operations, covering surface roughness, tool wear, wear mechanisms, and tool life. A mathematical model was developed to estimate metal cutting parameters for turning SUS 304 stainless steel using cemented tungsten-cobalt (WC-Co) coated carbide grade with Ti (C,N) + Al_2O_3 insert in two different turning environments employing MWF and MXene-NFC as the cutting fluid. When MXene-NFC was employed, parameter optimization was implemented to identify the optimal turning machining parameters, including cutting speed, feed rate, and depth of cut. The objective was to achieve the lowest surface roughness, longest tool life, and the greatest total length of cut. In summary, the study's findings and discussion highlight the notable advantages of MXene-NFC, emphasizing its potential for enhancing the efficiency and performance of turning operations in comparison to traditional MWF within the MQL cooling system as below:

a) In the milling process of SUS 304 with both MWF and MXene-NFC, it is observed that the surface roughness is influenced by the feed rate, depth of cut, and cutting speed. Notably, the turning operation with MXene-NFC yields a lower surface roughness value compared to the turning operation with MWF.

b) Operating at high cutting speeds during machining results in increased heat generation within the cutting zone. In a high-speed turning operation with MWF coolant, the cutting tool generates more heat compared to its counterpart utilizing MXene-NFC coolant. The elevated thermal conductivity of MXene-NFC serves as an effective thermal barrier, efficiently transporting a significant portion of the generated heat. This not only prolongs the tool life but also contributes to the production of finer surface finishes on workpieces.

c) The predominant modes of tool failure, observed during the machining of SUS 304 stainless steel with MWF, were flank wear and chipping.

d) In the machining of SUS 304, the observed tool wear mechanism on the coated carbide cutting tool primarily involved attrition or abrasion, adhesion, and diffusion. Notably, this investigation revealed the occurrence of build-up-edge (BUE) on the cutting tool.

e) In a turning operation utilizing MXene-NFC, the cutting tool requires approximately 50% more time to meet the ISO 3865:1997 wear requirements (0.3 mm) compared to when employing MWF. This leads to an extended length of cut for the workpiece.

f) Optimal machining parameters for MXene-NFC involve a cutting speed of 140 m/min, a feed rate of 0.05 mm/rev, and a depth of cut of 0.5 mm. These settings ensure minimal surface roughness, maximum tool life, and the greatest total length of cut, achieving a composite desirability of 0.695.

6.0 ACKNOWLEDGEMENT

The authors would like to thank UMP for funding this work under internal grant RDU223018.

7.0 REFERENCES

[1] B. Li, H.M. Zhu, C.J. Qiu, and D.K. Zhang, "Development of high strength and ductile martensitic stainless steel coatings with Nb addition fabricated by laser cladding," *Journal of Alloys and Compounds*, vol. 832, p. 154985, 2020.

[2] S.P. Chandrakant, and B. Patel, "A review on the effect of minimum quantity lubrication on different machining parameters emphasizing vegetable oil-based lubricants for sustainable manufacturing," *Advanced Materials Research*, vol. 1175, pp. 107-122, 2023.

[3] P. Sivaiah, D. Chakradhar, and R.G. Narayanan, "Sustainable manufacturing strategies in machining," *in Sustainable Manufacturing Processes 2023*, p. 113-154, Elsevier, 2023.

[4] Y. Guo, K. Li, D. Zou, Y. Li, L. Yan, Z. He, T. Zou, B. Huang, and P.K.L. Chan, "Large-area electrode deposition and patterning for monolayer organic field-effect transistors by vacuum-filtrated MXene," *Advanced Electronic Materials*, vol. p. 2300570, 2023.

[5] G. Gołda, and A. Kampa, "Modelling of cutting force and robot load during machining," *Advanced Materials Research*, vol. 1036, pp.715-720, 2014.

[6] T. Kitagawa, A. Kubo, and K. Maekawa, "Temperature and wear of cutting tools in high-speed machining of Inconel 718 and Ti 6Al 6V 2Sn," *Wear*, vol. 202, no. 2, pp. 142–148, 1997.

[7] V.P. Astakhov, and J.P. Davim, "Tools (Geometry and Material) and Tool Wear," *Machining*, Springer, London, 2008.

[8] D.A. Stephenson, and J.S. Agapiou, *Metal cutting theory and practice*, CRC Press, 2018.

[9] J. Lee, J. Kim, B. Seo, D. Shin, S. Hwang, and W. Choi, "Layer-by-layer solution-processed two-dimensional graphene oxide–polyethylenimine thin-film coatings for enhanced pool boiling heat transfer," *International Journal of Heat and Mass Transfer*, vol. 209, p. 124067, 2023.

[10] A. Nandakumar, T. Rajmohan, and S. Vijayabhaskar, "Experimental evaluation of the lubrication performance in MQL grinding of nano SiC reinforced Al matrix composites," *Silicon*, vol. 11, no. 6, pp. 2987-2999, 2019.

[11] N.R. Dhar, M.W. Islam, S. Islam, and M.A.H. Mithu, "The influence of minimum quantity of lubrication (MQL) on cutting temperature, chip and dimensional accuracy in turning AISI-1040 steel," *Journal of Materials Processing Technology*, vol. 171, no. 1, pp. 93-99, 2006.

[12] A. Jayal, G. Goindi, D. Mandal, S. Chavan, and P. Sarkar, "Investigation of ionic liquids as additives to canola oil in minimum quantity lubrication milling of plain medium carbon steel," *International Journal of Advanced Manufacturing Technology*, vol. 94, pp. 881–896, 2018.

[13] G.S. Goindi, A.D. Jayal, and P. Sarkar, "Application of ionic liquids in interrupted minimum quantity lubrication machining of plain medium carbon steel: Effects of ionic liquid properties and cutting conditions," *Journal of Manufacturing Processes*, vol. 32, p. 357-371, 2018.

[14] U. Sivakishore, and R. Venkatesh, "Utilizing CNC turning, compare the material removal rate for the novel alloy using a TiAlN-coated CS insert to an untreated CS insert," *Journal of Survey in Fisheries Sciences*, vol. 10, no. 1S, p. 1646-1656, 2023.

[15] M. Kumar, A.M. Sidpara, and V. Racherla, "Surface finishing of aluminium 6061 using fabricated flexible abrasive tool," *Materials Today Communications*, vol. 33, p. 104614, 2022.

[16] S. Wojciechowski, "Estimation of minimum uncut chip thickness during precision and micro-machining processes of various materials - A critical review," *Materials*, vol. 15, no. 1, pp. 59, 2022.

[17] L. Wan, D. Wang, and S. Wu, "The investigation of effects of friction on the formation of dead metal zone with finite element method," *International Journal of Internet Manufacturing and Services*, vol. 4, no. 2, pp. 118-133, 2016.

[18] D. Dudzinski, A. Devillez, A. Moufki, D. Larrouquere, V. Zerrouki, and J. Vigneau, "A review of developments towards dry and high speed machining of Inconel 718 alloy," *International Journal of Machine Tools and Manufacture*, vol. 44, no. 4, pp. 439-456, 2004.

[19] M.K. Gupta, P. Niesłony, M. Korkmaz, et al., "Potential use of cryogenic cooling for improving the tribological and tool wear characteristics while machining aluminum alloys," *Tribology International*, vol. 183, p. 108434, 2023.

[20] M. Mia, M.A. Bashir, M.A. Khan, and N.R. Dhar, "Optimization of MQL flow rate for minimum cutting force and surface roughness in end milling of hardened steel (HRC 40)," *The International Journal of Advanced Manufacturing Technology*, vol. 89, pp. 675-690, 2017.

[21] X. Wang, X. Ren, Y. Xue, and B. Luan, Investigation on Mircostructure and High Temperature Wear Properties of High-Speed Laser Cladding Inconel 625 Alloy. Accessed: Jan. 2023. [Online] Available at SSRN: https://ssrn.com/abstract=4604526.

[22] Z. Alam, F. Iqbal, and D.A. Khan, *Post-Processing Techniques for Additive Manufacturing*, CRC Press, 2023.

[23] A.A. Pasha, N. Islam, W. Jamshed, et al., "Statistical analysis of viscous hybridized nanofluid flowing via Galerkin finite element technique," *International Communications in Heat and Mass Transfer*, vol. 137, p. 106244, 2022.

[24] X.J. Wang, X.F. Li, Z.Z. Li, and F. Lin, "Investigation on dispersive behavior of TiO2-H2O Nanofluids," *Applied Mechanics and Materials*, vol. 468, pp. 49-52, 2013.

[25] M. Sharifpur, S. Yousefi, and J.P. Meyer, "A new model for density of nanofluids including nanolayer," *International Communications in Heat and Mass Transfer*, vol. 78, pp. 168-174, 2016.

[26] A.M. Hussein, R.A. Bakar, K. Kadirgama, and K. Sharma, "Experimental measurements of nanofluids thermal properties," *International Journal of Automotive and Mechanical Engineering*, vol. 7, pp. 850-863, 2013.

[27] S. Zhang, H. Ying, P. Huang, T. Yang, and W.-Q. Han, "Hierarchical utilization of raw Ti 3 C 2 T x MXene for fast preparation of various Ti 3 C 2 T x MXene derivatives," *Nano Research*, vol. 15, pp. 2746–2755, 2022.

[28] Y. Shao, L. Wei, X. Wu, et al., "Room-temperature high-precision printing of flexible wireless electronics based on MXene inks," Nature Communications, vol. 13, no. 1, p. 3223, 2022.

[29] L.S. Sundar, M.K. Singh, and A.C. Sousa, "Investigation of thermal conductivity and viscosity of Fe3O4 nanofluid for heat transfer applications," *International Communications in Heat and Mass Transfer*, vol. 44, pp. 7-14, 2013.

[30] M. Sandhya, D. Ramasamy, K. Kadirgama, W. Harun, and R. Saidur, "Assessment of thermophysical properties of hybrid nanoparticles [Graphene Nanoplatelets (GNPs) and Cellulose Nanocrystal (CNC)] in a base fluid for heat transfer applications," *International Journal of Thermophysics*, vol. 44, no. 4, p. 55, 2023.

[31] W. Azmi, K.A. Hamid, R. Mamat, K. Sharma, and M. Mohamad, "Effects of working temperature on thermo-physical properties and forced convection heat transfer of TiO2 nanofluids in water–Ethylene glycol mixture," *Applied Thermal Engineering*, vol. 106, pp. 1190-1199, 2016.

[32] M. Yogeswaran, K. Kadirgama, M. Rahman, and R. Devarajan, "Temperature analysis when using ethylene-glycol-based TiO2 as a new coolant for milling," *International Journal of Automotive and Mechanical Engineering*, vol. 11, no. 1, p. 2272-2281, 2015.

[33] M. Nalbant, H. Gökkaya, and G. Sur, "Application of Taguchi method in the optimization of cutting parameters for surface roughness in turning," *Materials & Design*, vol. 28, no. 4, pp. 1379-1385, 2007.

[34] T. Singh, V.K. Sharma, M. Rana, K. Singh, and A. Saini, "GRA based optimization of tool vibration and surface roughness in face milling of hardened steel alloy," *Materials Today: Proceedings*, vol. 50, pp. 2288-2293, 2022.

[35] T. Kaltenbrunner, H. Krückl, G. Schnalzger, et al., "Differences in evolution of temperature, plastic deformation and wear in milling tools when up-milling and down-milling Ti6Al4V," *Journal of Manufacturing Processes*, vol. 77, pp. 75-86, 2022.

[36] P. Stavroulakis, A.I. Toulfatzis, G.A. Pantazopoulos, and A.S. Paipetis, "Machinable leaded and eco-friendly brass alloys for high performance manufacturing processes: A critical review," *Metals*, vol. 12, no. 2, p. 246, 2022.

[37] M. Alauddin, M. El Baradie, and M. Hashmi, "Prediction of tool life in end milling by response surface methodology," *Journal of Materials Processing Technology*, vol. 71, no. 3, pp. 456-465, 1997.

[38] S. Wojciechowski, and P. Twardowski, "Tool life and process dynamics in high speed ball end milling of hardened steel," *Procedia Cirp*, vol. 1, p. 289-294, 2012.

[39] P. Koshy, R. Dewes, and D. Aspinwall, "High speed end milling of hardened AISI D2 tool steel (~ 58 HRC)," *Journal of Materials Processing Technology*, vol. 127, no. 2, pp. 266-273, 2002.

[40] C. Che-Haron, "Tool life and surface integrity in turning titanium alloy," *Journal of Materials Processing Technology*, vol. 118, no. 1-3, pp. 231-237, 2001.

[41] P. Dearnley, and A. Grearson, "Evaluation of principal wear mechanisms of cemented carbides and ceramics used for machining titanium alloy IMI 318," *Materials Science and Technology*, vol. 2, no. 1, pp. 47-58, 1986.

[42] P. Bhatia, P. Pandey, and H. Shan, "Failure of cemented carbide tools in intermittent cutting," *Precision Engineering*, vol. 1, no. 3, pp. 148-152, 1979.

[43] V.P. Astakhov, "Machining of hard materials–definitions and industrial applications," *In: Davim, J. (eds) Machining of Hard Materials*, Springer, London, 2011.

[44] B. Juneja, *Fundamentals of metal cutting and machine tools*, New Age International, 2003.

[45] S.S. Murshed, C.N. De Castro, M. Lourenço, M. Lopes, and F. Santos, "A review of boiling and convective heat transfer with nanofluids," *Renewable and Sustainable Energy Reviews*, vol. 15, no. 5, pp. 2342-2354, 2011.

[46] M.A. Xavior, and M. Adithan, "Determining the influence of cutting fluids on tool wear and surface roughness during turning of AISI 304 austenitic stainless steel," *Journal of Materials Processing Technology*, vol. 209, no. 2, pp. 900-909, 2009.

[47] A. Altin, M. Nalbant, and A. Taskesen, "The effects of cutting speed on tool wear and tool life when machining Inconel 718 with ceramic tools," *Materials & Design*, vol. 28, no. 9, pp. 2518-2522, 2007.

[48] A. Roy, and M. Banerjee, "A review study on graphene and hexagonal boron nitride," *International Journal of Research and Analytical Review*, vol. 9, no. 1, pp. 904-912, 2022.

[49] V. Vasu, and G. P. K. Reddy, "Effect of minimum quantity lubrication with Al2O3 nanoparticles on surface roughness, tool wear and temperature dissipation in machining Inconel 600 alloy," *Proceedings of the Institution of Mechanical Engineers, Part N: Journal of Nanoengineering and Nanosystems*, vol. 225, no. 1, pp. 3-16, 2011.

[50] A. Del Olmo, L.L. de Lacalle, G.M. de Pissón, et al., "Tool wear monitoring of high-speed broaching process with carbide tools to reduce production errors," *Mechanical Systems and Signal Processing*, vol. 172, p. 109003, 2022.

[51] P. Chakraborty, S. Asfour, S. Cho, A. Onar, and M. Lynn, "Modeling tool wear progression by using mixed effects modeling technique when end-milling AISI 4340 steel," *Journal of Materials Processing Technology*, vol. 205, no. 1-3, pp. 190-202, 2008.

[52] K. Abou-El-Hossein, and Z. Yahya, "High-speed end-milling of AISI 304 stainless steels using new geometrically developed carbide inserts," *Journal of Materials Processing Technology*, vol. 162, p. 596-602, 2005.

[53] G. Ibrahim, G., C.C. Haron, and J. Ghani, "The effect of dry machining on surface integrity of titanium alloy SUS 304 ELI," *Journal of Applied Sciences*, vol. 9, no. 1, pp. 121-127, 2009.

[54] A. Jawaid, S. Sharif, and S. Koksal, "Evaluation of wear mechanisms of coated carbide tools when face milling titanium alloy," *Journal of Materials Processing Technology*, vol. 99, no. 1-3, pp. 266-274, 2000.

[55] A.E. Diniz, Á.R. Machado, and J.G. Corrêa, "Tool wear mechanisms in the machining of steels and stainless steels," *The International Journal of Advanced Manufacturing Technology*, vol. 87, pp. 3157-3168, 2016.

[56] S. Karagöz, H. Fischmeister, H.-O. Andrén, and C. Guang-Jun, "Microstructural changes during overtempering of high-speed steels," *Metallurgical Transactions A*, vol. 23, pp. 1631-1640, 1992.

[57] W. König, R. Fritsch, and D. Kammermeier, "Physically vapor deposited coatings on tools: performance and wear phenomena," *Surface and Coatings Technology*, vol. 49, no. 1-3, pp. 316-324, 1991.

[58] E. Paul, C.J. Evans, A. Mangamelli, M.L. McGlauflin, and R.S. Polvani, "Chemical aspects of tool wear in single point diamond turning," *Precision Engineering*, vol. 18, no. 1, pp. 4-19, 1996.